Curved Glide-Reflection Symmetry Detection

Seungkyu Lee[1] Yanxi Liu[1,2]
[1] Department of Computer Science and Engineering
[2] Department of Electrical Engineering
The Pennsylvania State University, University Park, PA 16802, USA
sklee@psu.edu yanxi@cse.psu.edu

Abstract

We generalize reflection symmetry detection to a curved glide-reflection symmetry detection problem. We propose a unifying, local feature-based approach for curved glide-reflection symmetry detection from real, unsegmented images, where the classic reflection symmetry becomes one of four special cases. Our method detects and groups statistically dominant local reflection axes in a 3D parameter space. A curved glide-reflection symmetry axis is estimated by a set of contiguous local straight reflection axes. Experimental results of the proposed algorithm on 40 real world images demonstrate promising performance.

1. Introduction

Symmetry or near-symmetry is ubiquitous in the world around us. Automatic detection of symmetry in natural and man-made objects has been a lasting research interest in computer vision and pattern recognition [13]. Reflection symmetry is one of the most common basic symmetries [18], that has been used in many different fields for various applications, from face analysis [12], vehicle detection [5] to medical image analysis [10].

There exists a large body of 2D/3D reflection symmetry detection algorithms in the computer vision literature, ranging from Euclidean reflection symmetry [9, 11], to affinely [4, 15] and perspectively distorted [1, 2, 6, 17] reflection symmetry detections.

In 1983, Kanade coined the term *skewed symmetry* [4] denoting reflection symmetry of an object going through global affine or perspective skewing. The detection of reflection symmetry, rigid or skewed, has dominated the symmetry detection literature in computer vision. Even recently, new algorithms are developed for partial or approximate Euclidean reflection symmetry detection in subsampled 3D data [11], and from un-segmented images directly [9]. The first quantitative evaluation paper on discrete symmetry detection algorithms [13] considers [9], a local feature-based method, one of the best state of the art reflection symmetry detection algorithms.

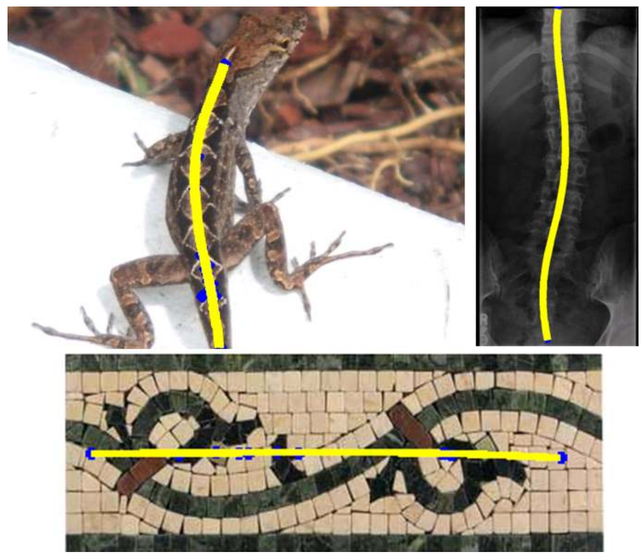

Figure 1: Curved (top) and straight (bottom) glide-reflection symmetry axes detected by the proposed algorithm (yellow lines)

However, when examining carefully, we can observe that many real world symmetrical objects/patterns do not present a classic reflection symmetry associated with a straight axis of reflection (Figure 1). Instead, they often have either a *curved reflection* axis or a *glide-reflection* symmetry – a primitive symmetry composed of a reflection and a translation along the direction of the reflection axis [18]. Except the algorithm in [7] determining glide-reflection symmetries for specific wallpaper/frieze symmetry group classifications, glide-reflection symmetry detection algorithms are rare. Glide-reflection with curved axis (Figure 1), the focus of this paper, has not been addressed computationally.

978-1-4244-3991-1/09/$25.00 ©2009 IEEE

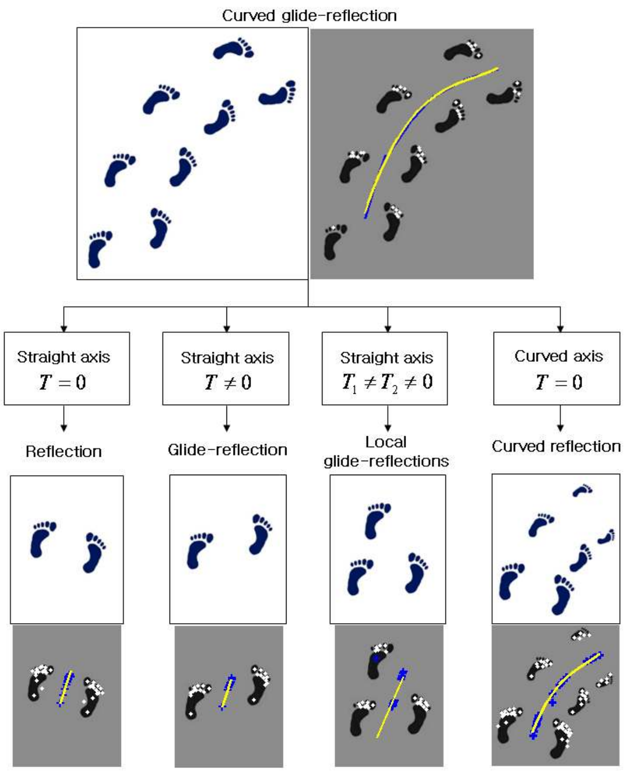

Figure 2: Four special cases of a curved glide-reflection symmetry and their detected axes by the proposed algorithm (yellow lines). Blue dots are the middle points of the supporting local feature pairs.

The curved reflection symmetry can often exist for a composed structure of multiple objects (Figure 2) that may not have a continuous closed contour thus quite different from medial axis, a topological skeleton of an object shape derived from the object contour [3]. Even for a connected body, medial axis may not always be consistent with the curved reflection symmetry axis of the texture on real objects (Figure 1). Peng et. al. [14] deals with the curved worm backbone detection and straightening problem, which is an application-specific, medial axis-based method.

The contributions of this paper include: (1) a conceptual generalization to *curved glide-reflection symmetries* such that reflection symmetry that has been dominating computer vision symmetry detection literature for the past 40 years becomes one of its four special cases; (2) a novel curved glide-reflection symmetry detection algorithm; (3) a test image set (40 images) and quantitative evaluations and an axis-straightening.

2. Curved Glide-Reflection Formalization

Glide-reflection is defined [18] as a symmetry composed of a translation T along and a reflection R about the same axis (Figure 2 bottom). Given a pair of image patches P_i, P_j with a glide-reflection symmetry, we have: $P_i = T + R(P_j)$. Thus, a pure reflection is a special case of a glide-reflection when $T = 0$. We can now define a *curved glide-reflection symmetry* as: a sequential collection of local glide-reflection symmetries whose reflection axes are connected and tangent to a smooth curve. Thus a curved, glide-reflection symmetry can be expressed as a sequence of (T_i, R_i)s where in general $T_i \neq T_j$ and $R_i \neq R_j$. The four special cases (Figure 2) are:

- (1) *Reflection* when T=0;
- (2) *Glide-reflection* when $T \neq 0$;
- (3) *Local glide-reflections* when multiple glide-reflections exist, and $T_1 \neq T_2$, and $T_1 \neq 0, T_2 \neq 0$;
- (4) *Curved reflection* when multiple reflections exist, $T_1 = T_2 = 0, R_1 \neq R_2$.

3. Glide-Reflection Detection

Our symmetry detection algorithm is a local feature point based matching method [9]. A feature point P_i is represented by its location x_i, y_i, orientation ϕ_i and scale s_i. Given a set of detected feature points, all possible pairs of feature points are investigated to find the reflection symmetry matches based on the local feature descriptor K_i. The orientation of the reflection axis is calculated from the orientations of a pair of matched points. After that, we calculate the amount of orientation deviation of the two matched feature points to find the translation T of the glide-reflection symmetry.

3.1. Feature Point Detection

Feature points-based matching allows efficient correspondence detection by investigating local feature points rather than the whole input image. The selection of the feature points is critical to our proposed algorithm performance. If only a small number of feature points are found from the input image or corresponding feature points are not found robustly, we will only have a weak cue to support a reflection symmetry. In our experiments, we use the SIFT [8] feature point matching. Though SIFT detects distinctive points robustly with good repeatability [9], SIFT key points are only detected at local maxima or minima locations, which are rarely found on a low-textured image with gradual change of intensity. Thus we propose to use several additional image filters before performing the key point detection, such as gradient and Canny edge detector. These filtered images create additional key points from local regions where key points were not detected using SIFT in the original intensity image (Figure 3). As a result, we achieve more potential matching pairs for symmetry detection.

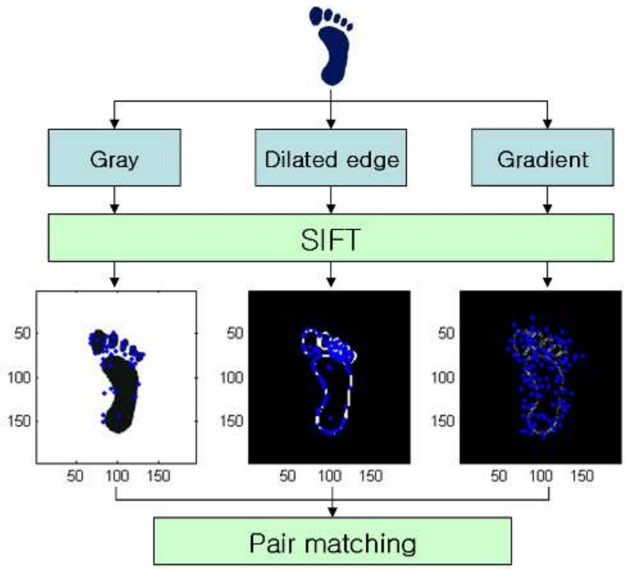

Figure 3: Feature points detection from the three different filtered inputs

Any other feature point detection method also can be applied for better matching pairs detection as long as it provides the feature descriptor, orientation and scale of the feature point.

3.2. Matching Pairs Selection

Given SIFT feature points and their local descriptor vectors, we compare all possible pairs of orientation normalized feature points. If two orientation normalized feature points exhibit a glide-reflection symmetry, the descriptor vector of one point matches with the mirrored descriptor vector of the other point. Similarity for matching is quantified by the Euclidean distance between the SIFT descriptors. After we sort the similarity of pairs at each feature point, we take the top 3 as the matched pairs at each feature points. At this step, the translation component T of the two feature points is not in consideration (Figure 4). Both (P_i, P_j) and (P_k, P_j) pairs will be dealt with as the same symmetry matches, which correspond to perfect reflection symmetry and glide-reflection symmetry respectively sharing the same reflection axis. In [9], glide-reflection pairs like (P_k, P_j) are penaltized. In our algorithm, we deal with both glide-reflection and reflection symmetries uniformly while the transformation T value tells them apart.

Once we find all best matching pairs for each feature point, we characterize the glide-reflection symmetry of them. Let $P_i = (x_i, y_i, \phi_i, s_i)$ and $P_j = (x_j, y_j, \phi_j, s_i)$ be two feature points (Figure 5). ϕ_i, ϕ_j and ϕ_{ij} are the orientation values of two key points and the line connecting them. If the two points of a matched pair form a glide-reflection symmetry, the orientation of its axis, ϕ_{axis}, is simply the

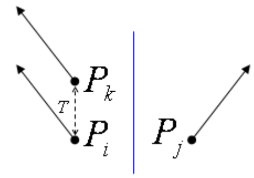

Figure 4: Reflection symmetry pair (P_i, P_j) (T=0) versus glide-reflection symmetry pair (P_k, P_j) ($T \neq$0)

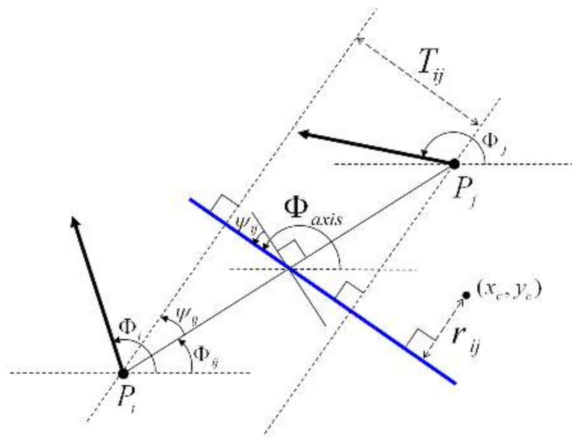

Figure 5: The orientation of the glide-reflection axis ϕ_{axis} and translation T_{ij}

average of the orientations of the two key points.

$$\phi_{axis} = \frac{\phi_i + \phi_j}{2} = \phi_{ij} + \psi_{ij} + \frac{\pi}{2} \tag{1}$$

Where ψ_{ij} is the deviation angle of the glide-reflection axis from the perpendicular line to the line connecting the two points (P_i and P_j). Then the translation T_{ij} can be calculated from the following equation.

$$T_{ij} = d_{ij} sin(\psi_{ij}) = d_{ij} sin(\frac{\phi_i + \phi_j - \pi}{2} - \phi_{ij}) \tag{2}$$

where, $d_{ij} = \sqrt{(x_i - x_j)^2 + (y_i - y_j)^2}$ is the distance between the two points. We also calculate the distance r_{ij} from the image center (x_c, y_c) to the glide-reflection axis.

$$r_{ij} = (\frac{x_i + x_j}{2} - x_c) sin\phi_{axis} - (\frac{y_i + y_j}{2} - y_c) cos\phi_{axis} \tag{3}$$

Now we can express our glide-reflection symmetry specifically as $P_i = T_{ij} + R_{r_{ij}, \phi_{axis}}(P_j)$, where $R_{r_{ij}, \phi_{axis}}$ is the reflection mapping with the reflection axis (r_{ij}, ϕ_{axis}). Given the specific form of the three dimensional parameter space for glide-reflection symmetries, we construct and analyze the 3D distribution of the three glide-reflection parameters detected in real images. Each matched pair (P_i and P_j) in the 3D parameter space is weighted by the product of the scaling S_{ij} and distance D_{ij} components as follows [9]:

$$M_{ij} = S_{ij} \times D_{ij}$$
$$= exp(\frac{-|s_i - s_j|}{s_i + s_j}) \times exp(\frac{-d_{ij}^2}{2max(d_{ij})}) \quad (4)$$

Feature point pairs of similar size and shorter distance get higher weights than others. This 3D parameter space distribution is convolved with a Gaussian kernel to build the density plot. Local maximum points indicate dominant axes. If the glide-reflection axis of input image is straight, the voting in the 3D parameter space should be centered around a point-like local maxima in (r_{ij}, ϕ_{axis}).

Figure 6 shows the 3D parameter space examples of the four cases of glide-reflection symmetries. Reflection is detected near $T_{ij} = 0$ (red circle of Figure 6 (a)). Glide-reflection has single non-zero T_{ij} value (red circle of Figure 6 (b)) while locally deformed glide-reflection has multiple (two) non-zero T_{ij} values (One is positive and the other is negative in Figure 6 (c)). In Figure 6 (d), three local maximum locations on the $T_{ij} = 0$ plane support a curved reflection axis connecting three local reflection symmetries. These special cases form the basic building blocks for the general curved glide-reflection symmetry case.

4. Curved Reflection Axis Detection

From an unsegmented image without any previous knowledge, we need to extract all potential local corresponding matches for glide-reflection symmetry. When the glide-reflection axis is curved, the axis does not appear as a single point in the 3D parameter space, as it does with a straight axis case. A curved axis is considered as a sequence of short straight glide-reflection axes having different yet smoothly varying orientations and different translation Ts. Therefore, a curved axis can be estimated by a set of contiguous points in the 3D parameter space. Based on the detected local glide-reflection matches, our algorithm seeks a set of local axes supporting a curved glide-reflection symmetry.

4.1. Axes Grouping in 3D Parameter Space

In real world images, multiple local straight glide-reflection axes of different orientations and Ts form a single curved glide-reflection. Figure 7 (b) shows seven local axes (yellow lines) supporting a curved axis detected by our algorithm (Figure 7 (f)). First we analyze reflection symmetry axes density in the 3D parameter space (Figure 7 (c)). We find the local maximum points on this 3D parameter space density which gives seven local axes. Each red circled set of matching pairs in Figure 7 (c) corresponds to each local axis shown in 7 (b). Note that they have two different types of translation components (T_a and T_b) which can be clearly detected in our 3D parameter space (Figure 7 (c)). After that, local axes near (with respect to the Euclidean distance of (r_{ij}, ϕ_{axis}) coordinate) each other are grouped. This can be done in a 2D density plot (Figure 7 (d)) obtained by cumulating points along the T-axis of the 3D parameter space density. As a result, we find a series of local straight axes having contiguous r_{ij} and ϕ_{axis} values. Figure 7 (e) shows a detected axes group corresponding to a curved glide reflection axis in Figure 7 (f).

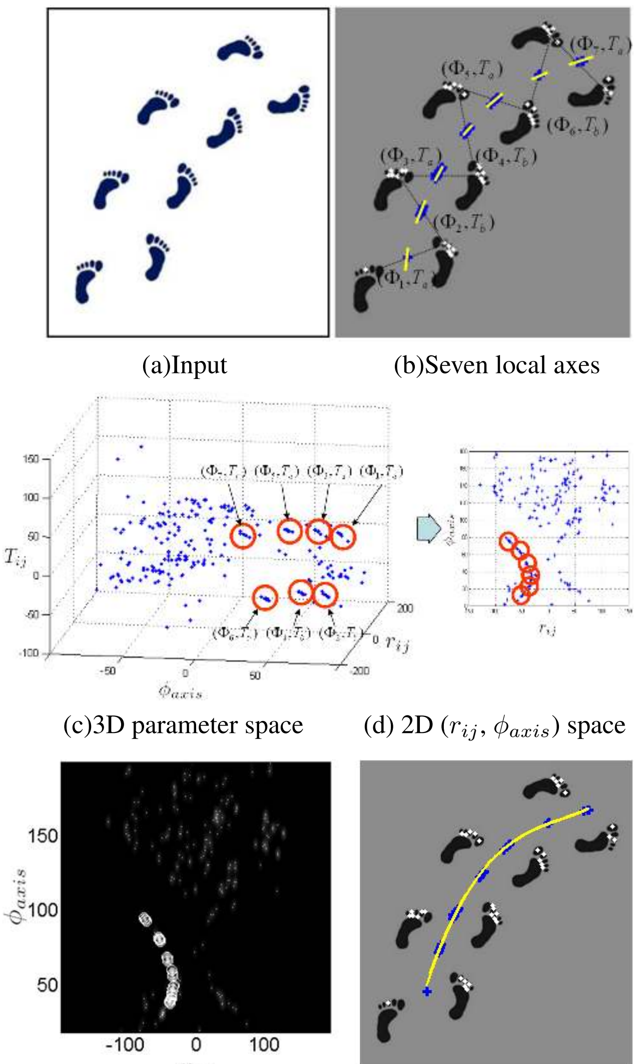

(a)Input (b)Seven local axes

(c)3D parameter space (d) 2D (r_{ij}, ϕ_{axis}) space

(e)2D density (f)Output

Figure 7: An example of curved glide-reflection axis detection: Blue points in (b) are middle points of supporting matched pairs for each local axis. Yellow lines are local axes. 3D parameter space (c) shows each detected local axis (red circled). They have two different types of translation components (T_a and T_b) which are shown in (b).

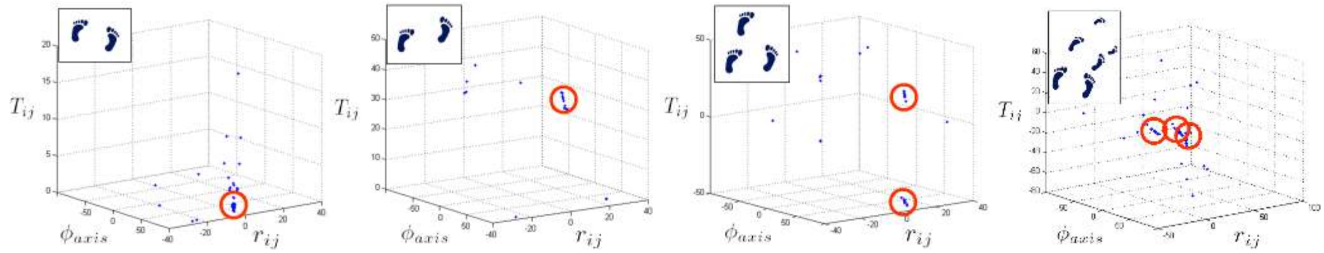

(a) Reflection (b) Glide-reflection (c) Local glide-reflections (d) Curved reflection

Figure 6: 3D parameter space examples of the four sub types of curved glide-reflection symmetries: Red circles show the characteristic patterns detected in the 3D parameter space location.

Method	Detection rate	Processing time*
Loy and Eklundh [9]	7.5%	6.6(9.8)sec
Peng et. al. [14]	0.0%	75.0(220.5)sec
Proposed	70.0%	9.9(11.5)sec

Table 1: Quantitative experimental results. $*$ Mean (standard deviation) processing time of 40 images (See all results in the supplemental material)

4.2. Curve Fitting

Given all local axes detected in the 3D parameter space supporting a curved glide reflection axis, we can locate the middle points m_k of all supporting feature point pairs of the local axes back in the spatial domain. White points in Figure 7 (b) represent the feature point pairs supporting the selected axes. Blue points in Figure 7 (b) are the middle points m_k of supporting feature point pairs. By connecting all middle points, we can get a curved glide-reflection axis. However, the algorithm does not guarantee that the detected middle points are dense enough to find the correct glide-reflection axis. To achieve a smooth and precise curved axis, we use a regression method for curve fitting given the middle point set m_k. In our algorithm, we fit polynomial curves of the degree c varying from 1 to 5. Each degree of the polynomial has four orientations ($r = 0^o$, 45^o, 90^o and 135^o). We calculate the summation of distance $S(c_i, r_j) = \sum_{k=1}^{N} d_{ij}(k)$ where $d_{ij}(k)$ is the distance from the m_k to the polynomial of (c_i, r_j)). Among the total 20 polynomial curves (5 degrees $\times$ 4 orientations), the one having the lowest distance S from all middle points is selected as the final curved axis ($(c_{fit}, r_{fit}) = \arg\min_{c_i, r_j} S(c_i, r_j)$).

5. Experimental Results

We test our algorithm on the 40 various images of leaves, reptiles, fishes and spinal x-ray images. Table 1 shows the detection rate and mean processing time compared to the two previous methods [9] [14]. All methods are coded by Matlab and run on the Windows XP, 3.2GHz Pentium CPU. The processing time of the proposed algorithm mainly dependent upon the number of detected feature points varying from hundreds to thousands. Detailed experimental results and potential applications of the proposed algorithm are explained in the following sections with Figure 8, 10, 11, 12 and 13.

5.1. Curved Glide-Reflection Detection

Figure 12 shows straight glide-reflection axes detection on some synthetic wall paper images. Figure 13 shows experimental result on real world images. We find the curved reflection symmetries at leaves or trunks (Figure 13 (a), (d), (e) and (f)). Figure 13 (c) is a lizard with a reflection symmetry pattern on its back. This is a good example having a medial axis and reflection axis at different locations. Figure 13 (h) is vertical cut image of a zebra fish. Inside tissue of the fish supports the curved reflection axis. Left part of the detected axis in Figure 13 (d) is inaccurate due to a middle point outlier. Figure 13 (j) is a failure result due to its complicated background clutters. In Figure 13 (k), not enough key point matches are found to support the whole curved axis.

5.2. Axis Curvature Detection

One application of our algorithm is the detection of the curved spine axis from the x-ray images. Figure 8 shows several curved spine axis detection results of the Scoliosis spine x-ray images. When they diagnose the Scoliosis, the curvature of the spine plays an important role. Our algorithm can detect the curvature of the spine automatically by investigating the parameterized curve fitted on the curved spine in an X-ray image.

5.3. Curved Axis Straightening & Recognition

Once we find the curved glide-reflection axis with the parameterized axis model, we can calculate the curvature

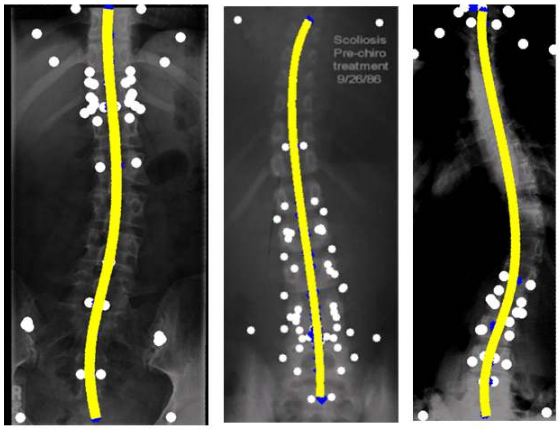

Figure 8: Experimental results on the Scoliosis X-ray spine images. Detected axis of the rightmost image is not accurate because of the lack of supporting feature point pairs.

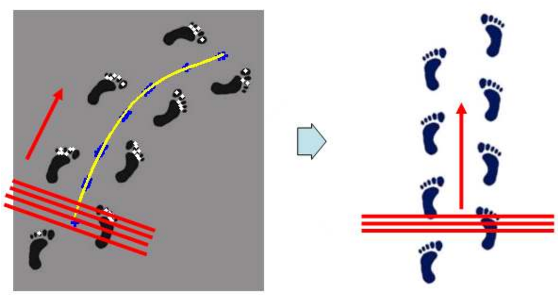

Figure 9: Curved axis straightening

at any location on the curve. Based on the curvature information at each location, we can recover the straight axis by realigning each normal line of the curved axis vertically (Figure 9).

Figure 10 shows two examples of the curved axis straightening. Figure 10 (a) is a leaf from the Swedish leaf database [16]. Original leaf image has curved reflection axis. Curve on the axis is not an innate nature of the leaf and introduces noise on the shape description of the leaf. After automatic curved axis detection by the proposed algorithm we can straighten the original image. This process is a type of normalization along the reflection axis and may increase the leaf recognition performance. Any other shape recognition method of the deformable objects can benefit from straightening them along the reflection axes. This may lead to the quantification of the deformation for further description of the shape. Figure 10 (b) is another example with a spine x-ray image from the previous section.

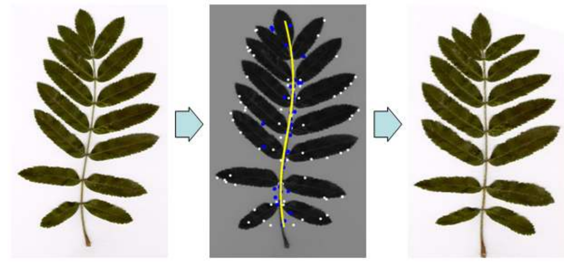

(a) Swedish leaf

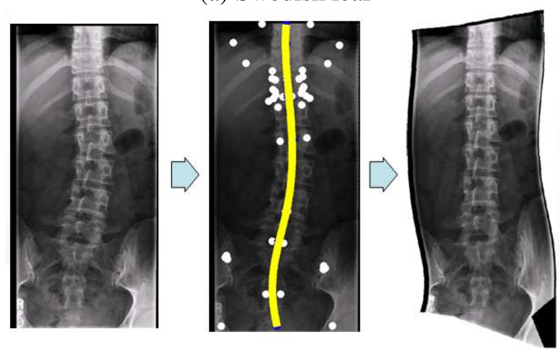

Input Curved axis Straightened

(b) Scoliosis spine

Figure 10: Curved axis straightening examples

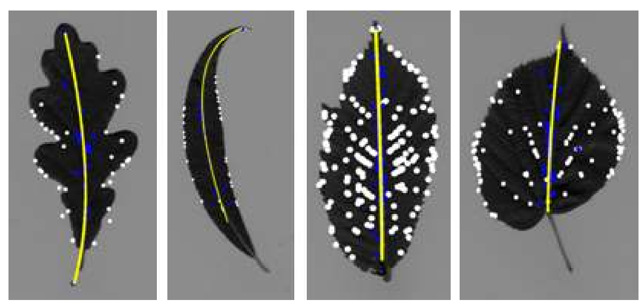

Figure 11: Curved axis detection on the Swedish leaves [16]

6. Discussion & Conclusion

We generalize the traditional reflection symmetry concept to curved glide-reflection symmetries that populate the real world, especially in biomedical image data. We propose a feasible algorithm based on local feature extraction and parameter subspace matching. We have evaluated our algorithm using a 40-real-image test set with 70% success rate. The proposed algorithm has a $O(N_f^2)$ complexity where N_f is the number of feature points. Though the proposed algorithm shows promise, there is plenty of room for improvements. First of all, like all feature-based methods the performance of our algorithm suffers if the feature point extraction step fails. So a more effective and versatile interesting-feature extractor is needed. The proposed

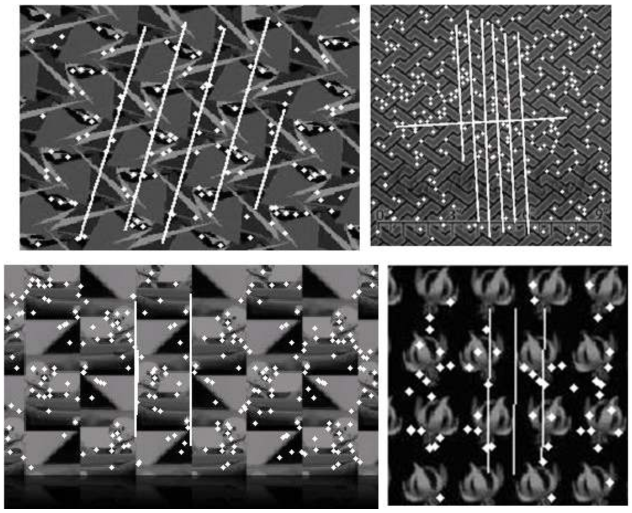

Figure 12: Glide-reflection axes detection on wallpaper patterns.

algorithm can deal with affine or perspective skewing of a curved glide-reflection symmetry as long as the feature is invariant to affine or perspective transformation. Second, the grouping method in our 3D parameter space favors bigger and longer curved axes supported by more feature point pairs. This strategy occasionally eliminates small, weak but true curved symmetries. Hierarchical approaches can be adopted to address this problem. Finally, outlier middle points at the polynomial curve fitting step can distract the fitted curve from the ground truth. A better regression method and an outlier elimination method can improve the curve fitting performance. The outcome of our proposed algorithm can be used for image matching, curvature detection in biomedical images and object recognition.

Acknowledgement

We thank Loy and Eklundh [9] and Peng et. al. [14] for their respective source code, Dr. K. C. Cheng for the Zebrafish images. This work is supported in part by an PSU CTSA grant.

References

[1] S. Carlsson. Symmetry in perspective. In *European Conference on Computer Vision vol.1*, pages 249–263, 1998.

[2] H. Cornelius and G. Loy. Detecting bilateral symmetry in perspective. In *Proceedings of International Conference on Computer Vision and Pattern Recognition Workshop*, page 191, 2006.

[3] D. A. Forsyth and J. Ponce. *Computer Vision: A Modern Approach*. Prentice Hall, August 2002.

[4] T. Kanade and J. R. Kender. Mapping image properties into shape constraints: skewed symmetry, affine-transformable patterns, and the shape-from-texture paradigm. In *Human and Machine Vision*, pages 237–257. Academic Press, 1983.

[5] A. Kuehnle. Symmetry-based recognition of vehicle rears. *Pattern Recogn. Lett.*, 12(4):249–258, 1991.

[6] Y. Lei and K. Wong. Detection and localisation of reflectional and rotational symmetry under weak perspective projection. *Pattern Recognition*, 32(2):167–180, 1999.

[7] Y. Liu, R. Collins, and Y. Tsin. A computational model for periodic patern perception based on frieze and wallpaper groups. *IEEE Transactions on Pattern Analysis and Machine Intelligence*, 26(3):354–371, 2004.

[8] D. G. Lowe. Distinctive image features from scale-invariant keypoints. *International Journal of Computer Vision*, 60:91–110, 2004.

[9] G. Loy and J. Eklundh. Detecting symmetry and symmetric constellations of features. In *European Conference on Computer Vision*, pages II: 508–521, 2006.

[10] M. Mancas, B. Gosselin, and B. Macq. Fast and automatic tumoral area localisation using symmetry. *IEEE International Conference on Acoustics, Speech, and Signal Processing.*, 2:725–728, 18-23, 2005.

[11] N. J. Mitra, L. J. Guibas, and M. Pauly. Partial and approximate symmetry detection for 3d geometry. *ACM Trans. Graph.*, 25(3):560–568, 2006.

[12] S. Mitra and Y. Liu. Local facial asymmetry for expression classification. In *Proceedings of International Conference on Computer Vision and Pattern Recognition*, volume 2, pages 889 – 894, June 2004.

[13] M. Park, S. Lee, P.-C. Chen, S. Kashyap, A. A. Butt, and Y. Liu. Performance evaluation of state-of-the-art discrete symmetry detection algorithms. In *Proceedings of IEEE International Conference on Computer Vision and Pattern Recognition*, pages 1–8, June 2008.

[14] H. Peng, F. Long, X. Liu, S. K. Kim, and E. W. Myers. Straightening c. elegans images. *Bioinformatics*, pages btm569+, November 2007.

[15] D. Shen, H. Ip, and E. Teoh. Robust detection of skewed symmetries. In *International Conference on Pattern Recognition*, pages 1010–1013, 2000.

[16] O. J. O. Söderkvist. Computer vision classification of leaves from swedish trees. Master's thesis, Linköping University, SE-581 83 Linköping, Sweden, September 2001. LiTH-ISY-EX-3132.

[17] L. Van Gool, M. Proesmans, and T. Moons. Mirror and point symmetry under perspective skewing. In *Proceedings of International Conference on Computer Vision and Pattern Recognition*, pages 285–292, 1996.

[18] H. Weyl. *Symmetry*. Princeton University Press, 1952. ISBN 0-691-02374-3.

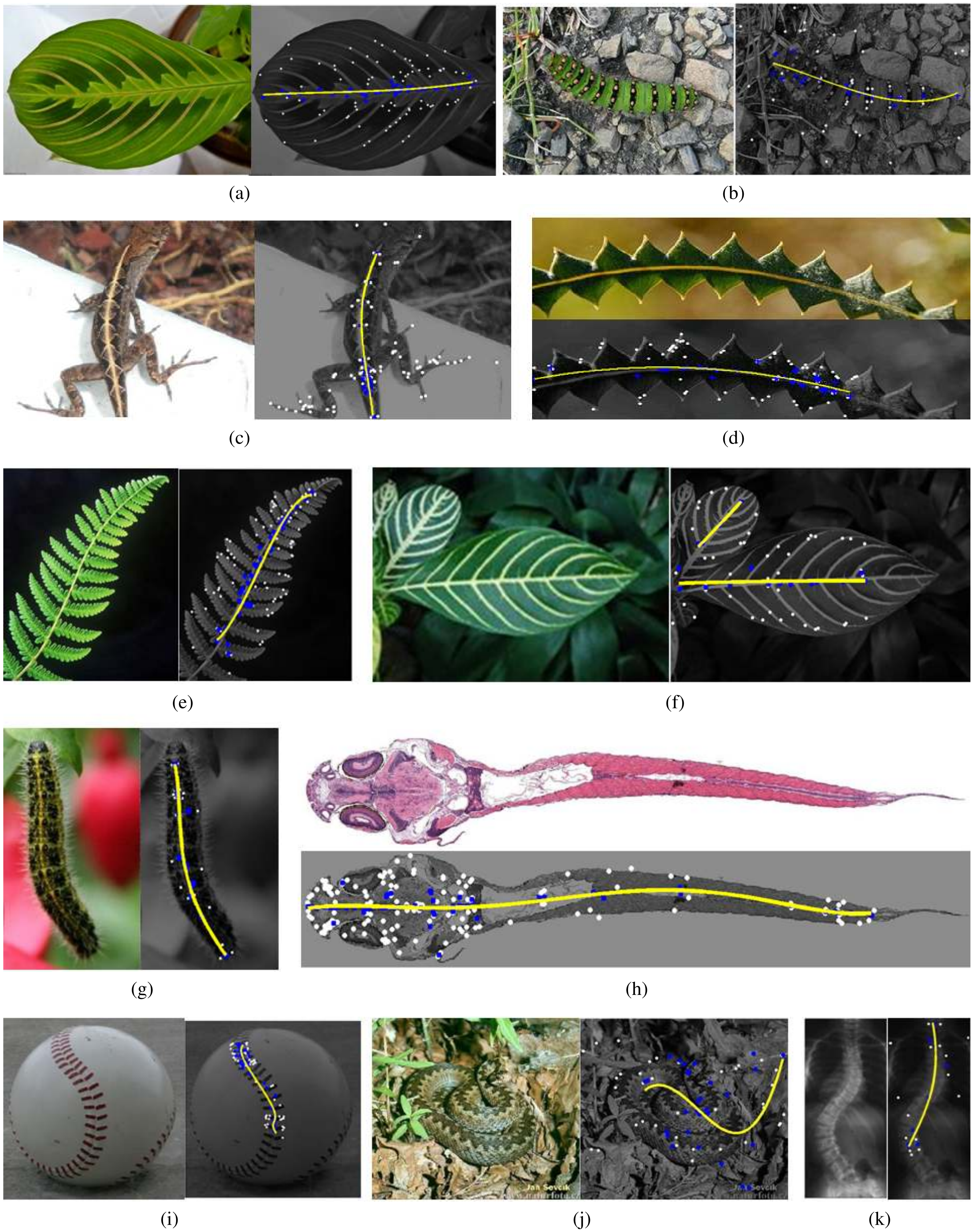

Figure 13: Experimental results on real-world images